Inorganic Chemistry

Article

pubs.acs.org/IC

Antitumoral, Antihypertensive, Antimicrobial, and Antioxidant Effects of an Octanuclear Copper(II)-Telmisartan Complex with an Hydrophobic Nanometer Hole

María S. Islas,[†] Juan J. Martínez Medina,[‡] Libertad L. López Tévez,[‡] Teófilo Rojo,[§] Luis Lezama,[§] Mercedes Griera Merino,[∥] Laura Calleros,[∥] María A. Cortes,[∥] Manuel Rodriguez Puyol,[∥] Gustavo A. Echeverría,[⊥] Oscar E. Piro,[⊥] Evelina G. Ferrer,[†] and Patricia A. M. Williams*[,†]

[†]Centro de Química Inorgánica (CEQUINOR/CONICET/UNLP)- Facultad de Ciencias Exactas, Universidad Nacional de La Plata, 47 esq. 115, 1900 La Plata, Argentina

[‡]Departamento de Química, UNCAUS, Cte. Fernández 755 (3700), Roque Saénz Peña, Chaco, Argentina

[§]Departamento de Química Inorgánica, Facultad de Ciencia y Tecnología, Universidad del País Vasco, Apdo. 644, 48080 Bilbao, Spain

[∥]Departamento de Fisiología, Universidad de Alcalá, Campus Universitario, 28871 Alcalá de Henares, Madrid, Spain

[⊥]Departamento de Física, Facultad de Ciencias Exactas, Universidad Nacional de La Plata- Institute IFLP (CONICET, CCT-La Plata), C. C. 67, 1900 La Plata, Argentina

S *Supporting Information*

ABSTRACT: A new Cu(II) complex with the antihypertensive drug telmisartan, $[Cu_8Tlm_{16}]\cdot 24H_2O$ (CuTlm), was synthesized and characterized by elemental analysis and electronic, FTIR, Raman and electron paramagnetic resonance spectroscopy. The crystal structure (at 120 K) was solved by X-ray diffraction methods. The octanuclear complex is a hydrate of but otherwise isostructural to the previously reported $[Cu_8Tlm_{16}]$ complex. $[Cu_8Tlm_{16}]\cdot 24H_2O$ crystallizes in the tetragonal *P*4/*ncc* space group with $a = b = 47.335(1)$, $c = 30.894(3)$ Å, $Z = 4$ molecules per unit cell giving a macrocyclic ring with a double helical structure. The Cu(II) ions are in a distorted bipyramidal environment with a somewhat twisted square basis, *cis*-coordinated at their core N_2O_2 basis to two carboxylate oxygen and two terminal benzimidazole nitrogen atoms. Cu_8Tlm_{16} has a toroidal-like shape with a hydrophobic nanometer hole, and their crystal packing defines nanochannels that extend along the crystal *c*-axis. Several biological activities of the complex and the parent ligand were examined *in vitro*. The antioxidant measurements indicate that the complex behaves as a superoxide dismutase mimic with improved superoxide scavenger power as compared with native sartan. The capacity of telmisartan and its copper complex to expand human mesangial cells (previously contracted by angiotensin II treatment) is similar to each other. The antihypertensive effect of the compounds is attributed to the strongest binding affinity to angiotensin II type 1 receptor and not to the antioxidant effects. The cytotoxic activity of the complex and that of its components was determined against lung cancer cell line A549 and three prostate cancer cell lines (LNCaP, PC-3, and DU 145). The complex displays some inhibitory effect on the A549 line and a high viability decrease on the LNCaP (androgen-sensitive) line. From flow cytometric analysis, an apoptotic mechanism was established for the latter cell line. Telmisartan and CuTlm show antibacterial and antifungal activities in various strains, and CuTlm displays improved activity against the *Staphylococcus aureus* strain as compared with unbounded copper(II).

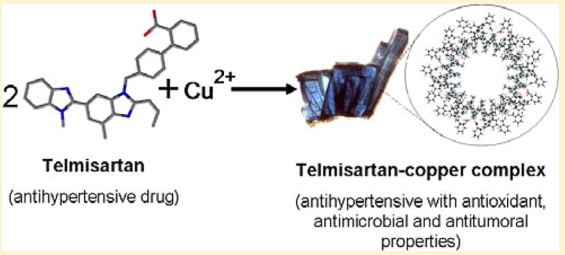

INTRODUCTION

Angiotensin II (AII), an octapeptide with the amino acid sequence Asp-Arg-Val-Tyr-Ile-His-Pro-Phe, is a very potent chemical that causes muscles to contract, thereby narrowing embedded blood vessels. This narrowing increases the blood pressure and can cause hypertension. Attempts to develop therapeutically useful AII receptor antagonists were focused on a series of imidazole-5-acetic acid derivatives. By use of rational drug design and molecular modeling techniques and through a clever series of stepwise modifications, these lead compounds later gave rise to orally active, potent, and selective nonpeptide AII receptor antagonists. At present, orally available sartans have been developed and are used to treat both hypertension and damage associated with diseases such as atherosclerosis and diabetes. AII sartans bind with a high affinity to the AII type 1 (AT1) receptor and share a common mechanism of action. Telmisartan (2-(4-{[4-methyl-6-(1-methyl-1H-1,3-benzodiazol-2-yl)-2propyl-1*H*-1,3-benzodiazol-1-yl]methyl}phenyl)benzoic acid) (Figure 1) displayed a highly selective and potent

Received: March 3, 2014

   dx.doi.org/10.1021/ic500483p | *Inorg. Chem.* XXXX, XXX, XXX–XXX

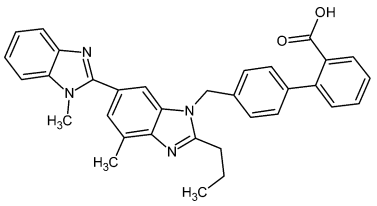

Figure 1. Telmisartan.

antagonism of the AT1 receptor in many tissues, including vascular smooth muscle and the adrenal gland, hence resulting in inhibition of the vasopressor and aldosterone secreting effects of AII. Taking into account that AII is a physiologically active major substance of the renin-angiotensin system (RAS), the inhibition of the RAS by angiotensin-converting enzyme inhibitors and/or AT1 receptor blockers (ARBs) or sartans may be a therapeutic target for organ protection in patients with hypertension, inhibiting the vasoconstrictor effects of AII. Besides, it was found that telmisartan has the strongest blood pressure lowering activity of all sartans.[1,2]

The control of blood pressure is not the only therapeutic effect of the ARBs. ARB-based therapy has cardioprotective, cerebroprotective, and renoprotective effects, including regression of left ventricular hypertrophy, reduction in stroke risk, and slowing of renal disease progression.[3,4] Some studies support the possibility that the consumption of an ARB as an anti-inflammatory agent might be able to be used to suppress the exacerbation of cytotoxic T-cell-mediated diseases such as myocarditis and renal transplantation rejections.[5] Studies in animal models have shown that blocking the actions of ATII with ARBs can be effective for preventing the progression of atherosclerosis.[6] Also, ARBs represent a potential novel and promising strategy for controlling angiogenesis, preventing metastasis, and prolonging survival in patients with primary or metastatic pancreatic ductal adenocarcinoma. There has been earlier evidence that ATII blockade therapies suppress tumor growth, metastases, and angiogenesis in experimental animal models and reduce cancer prevalence in hypertensive patients.[7]

Copper is an essential element that functions as a cofactor during aerobic metabolism; however, in low or excessive amounts copper can have deleterious effects. It is essential for cellular respiration, iron homeostasis, pigment formation, neurotransmitter production, peptide biogenesis, connective tissue biosynthesis, and antioxidant defense.[8,9] Currently, the antimicrobial properties of metallic copper surfaces are being tested against numerous pathogens. Additionally, the use of copper vessels for drinking water has been incorporated in developing countries as a low-cost alternative in the prevention of bacterial infections.[10,11]

On the other hand, it has been shown that the combination of hydrophobic ion pairs (HIPs) could be used for drug delivery and also allows the combination of two or more active pharmaceutical ingredients, resulting in a multifunctional release system. Dissociation of Cl_xLos_2 (HIPs of chlorhexidine and losartan) could provide a dual action drug for the treatment of heart diseases caused or intensified by microorganisms.[12] Moreover, the complex between losartan and hydroxypropil-β-cyclodextrin demonstrated efficiency in hypertension control within a long time interval (30 h), in comparison with losartan alone (6 h). These results indicate that complexation improves the extent and duration of Losartan antagonistic action.[13] In this context, it is interesting to note that the complexation of ARBs with some transition metals could be a useful strategy to develop novel antihypertensive drugs with enhanced properties such as antihypertensive, antioxidant, antitumoral, and antimicrobial activities. We have previously measured the antitumoral effects of losartan, valsartan, and their copper(II) complexes in osteoblasts.[14,15] Besides, the antioxidant properties through superoxidedismutase (SOD) mimetic activity determinations for losartan, candesartan, and their copper(II) complexes were determined.[14,16] Nevertheless, the *in vitro* antimicrobial activity of ARBs and their metal complexes has not been studied yet. In this paper we report the synthesis and structural characterization of a new coordination complex between copper(II) and telmisartan. We have also determined the antihypertensive effect of the complex in comparison with the parent sartan measuring the expanding effect of both compounds on mesangial contractile cells and their antioxidant and cytotoxic properties (against A549 human lung carcinoma cell line). The mechanism of the cytotoxic action was studied for the LNCaP prostate cancer cell line in which the highest sensitivity to the complex was determined. The antibacterial and antifungal profile of the novel sartan copper complex was also determined including candesartan and its complex for comparative purposes. Interestingly, the copper complex was able to improve the copper's inherent antimicrobial activity against the *Staphylococcus aureus* strain.

EXPERIMENTAL SECTION

Materials and Methods. All chemicals were of analytical grade and used without further purification. Copper(II) chloride dihydrate was purchased from Riedel de Häen, and pure commercial telmisartan (Hangzhou Garden Trading Co., Ltd. (China)) was used as supplied. Elemental analyses (EA) for carbon, hydrogen, and nitrogen were performed using a Carlo Erba EA 1108 analyzer. Thermogravimetric analysis (TGA) and differential thermal analysis (DTA) were performed with Shimadzu systems (models TG-50 and DTA-50, respectively), working in an oxygen flow of 50 mL/min and at a heating rate of 10 °C/min. Sample quantities ranged between 10 and 20 mg. Al_2O_3 was used as a differential thermal analysis standard. FTIR spectra of powdered samples (as pressed KBr pellets) were measured with a Bruker IFS 66 FTIR-spectrophotometer from 4000 to 400 cm^{-1}. FT-Raman spectra were measured using the FRA 106 Raman accessory. A continuous-wave Nd:YAG laser working at 1064 nm was employed for Raman excitation. A germanium detector operating at liquid nitrogen temperature was used. Diffuse reflectance spectra were registered with a Shimadzu UV-300 instrument, using MgO as an internal standard. Electronic absorption spectra were recorded on a Hewlett-Packard 8453 diode-array spectrophotometer, using 1 cm quartz cells. A Bruker ESP300 spectrometer operating at the X-band and Q-band and equipped with standard Oxford Instruments low-temperature devices (ESR900/ITC4) was used to record the electron paramagnetic resonance (EPR) spectrum of the complex at room temperature in the solid state and in dimethylformamide (DMF) solution at 140 K. A computer simulation of the EPR spectra was performed using the program SimFonia.[17]

Preparative. *$[Cu_8(Tlm)_{16}]\cdot 24H_2O$ (CuTlm).* A solution of $CuCl_2\cdot 2H_2O$ in ethanol (0.5 mmol, 5 mL) was added under continuous stirring to an ethanol solution of telmisartan (1 mmol, 10 mL). The obtained suspension was allowed to stir and was dissolved by the addition of an aqueous solution of 1 M NaOH. The final pH value was 7. The formation of a blue precipitate was observed following water (15 mL) addition. The resulting solid product was filtered off, washed with cold water, and then dried. When the solid was dissolved in ethanol blue single crystals suitable for structural X-ray diffraction studies were obtained in the mother liquor after 3 days. Yield: 0.484 g, 85%. Anal. Calc.%: C, 69.2; H, 5.6; N, 9.8. Exp.%: C, 69.0; H, 5.3; N, 9.7. Thermogravimetric analysis confirmed the presence of three labile water molecules per copper atom (Exp. loss: 4.6%. Calc. loss: 4.7%;

dx.doi.org/10.1021/ic500483p | Inorg. Chem. XXXX, XXX, XXX−XXX

broad endothermic peak, DTA, T 100 °C). At 800 °C the weight loss (93.1%, calc.; 93.2%, exp.) represents the formation of CuO that was characterized by FTIR spectroscopy. UV−visible spectrum (ethanol, powder and single crystal): 570 nm (ε, per copper atom = 9.4 M^{-1} cm^{-1}) and 720 nm (sh) (ε, per copper atom = 5.2 M^{-1} cm^{-1}). Diffuse reflectance spectrum (powder and single crystal): 592 and 720 nm (sh).

Crystal Data. A $[Cu_8Tlm_{16}]\cdot 24H_2O$ single crystal was extracted from the mother liquor, soaked with a synthetic oil drop, and then positioned within a nylon loop on top of a goniometer head before the sample was cooled to 120 K by blowing boiling nitrogen vapor with a cryostat device. The X-ray measurements were then performed on an Oxford Xcalibur Gemini, Eos CCD diffractometer with graphite-monochromated CuKα (λ = 1.54178 Å) radiation. X-ray diffraction intensities were collected (ω scans with ϑ and κ-offsets), integrated, and scaled with CrysAlisPro[18] suite of programs. The unit cell parameters were obtained by least-squares refinement (based on the angular settings for all collected reflections with intensities larger than seven times the standard deviation of measurement errors) using CrysAlisPro. Data were corrected empirically for absorption employing the multiscan method implemented in CrysAlisPro. The crystal diffracted poorly at high angles, and the data beyond 1.3 Å resolution showed that only less than half the observed intensities were above two standard deviations of experimental errors (in the 1.3−1.2 Å resolution interval, 32% of observed intensities; in the 1.2−1−1 Å range, 16.5% observed). This made difficult the standard *ab initio* structure solution and refinement. Though both Patterson and direct methods revealed the copper positions, it was not possible to develop reliably the full molecular structure by the usual procedure of alternated cycles of difference Fourier maps and least-squares refinement. At this stage, it was clear that the solid was a hydrate of but otherwise isostructural to the reported 0.93 Å resolution $[Cu_8Tlm_{16}]$ complex.[19] We therefore proceeded to refine the published molecular model against our 1.3 Å resolution diffraction data by full-matrix least-squares refinement with SHELXL-97.[20,21]

To reduce the number of parameters to be adjusted all but the copper atoms were refined with isotropic displacement parameters and the ligand phenyl groups fitted to regular hexagons with d(C−C) = 1.39 Å. Other C−C bond lengths and the C−N bond distances were restrained to target values of 1.44(2) and 1.32(2) Å, respectively. The tetrahedral bonding angles around the methylene C atoms on the pendant >C−CH_2−CH_2−CH_3 groups were ensured by restraining alternated C···C distances to a target value of 2.28(2) Å. A difference Fourier map phased on the non-H atoms of the refined $[Cu_2Tlm_4]$ content of the crystal asymmetric unit showed six crystallization water molecules which were incorporated to the model and refined isotropically. A further difference map phased on the $[Cu_2Tlm_4]\cdot 6H_2O$ model showed residual electron density due to severely disordered solvent which could not be modeled adequately in terms of atomic contributions, hence limiting the quality of the least-squares fitting (agreement R_1 factor equal to 0.329). Therefore, we proceeded with the refinement of the relatively ordered $[Cu_2Tlm_4]\cdot 6H_2O$ structure resorting to a described procedure[22] and implemented in the program SQUEEZE included in the PLATON[23] suite of programs. As a result, the overall quality of the refinement improved and the R_1 value dropped to 0.185. The ligand H atoms were then positioned on a stereochemical basis and refined with the riding model with the methyl groups at staggered positions. The water H atoms could not be located reliably, and therefore they were not included in the molecular model. Crystal data, data collection procedure, structure determination methods, and refinement results are summarized in Table 1. Crystallographic structural data have been deposited at the Cambridge Crystallographic Data Centre (CCDC). Any request to the CCDC for this material should quote the full literature citation and the reference number CCDC 987885.

Spectrophotometric Titrations. The molar ratio method was used to establish the stoichiometry of the complexes in solution. The absorption spectra of different ethanol solutions of 0.00625 M telmisartan with or without $CuCl_2\cdot 2H_2O$ were measured. In both cases ligand-to-metal molar ratios from 10 to 1.2 were used, and the pH values were adjusted to 7 with solid sodium methoxide.

Table 1. Crystal Data and Structure Refinement Results for $[Cu_8Tlm_{16}]\cdot 24H_2O$

empirical formula	$C_{528}H_{488}Cu_8N_{64}O_{56}$
formula weight	9134.14
temperature	120(2) K
wavelength	1.54184 Å
crystal system	tetragonal
space group	$P4/ncc$ (No. 130)
unit cell dimensions	a = 47.335(1) Å
	b = 47.335(1) Å
	c = 30.894(3) Å
volume	69221(7) $Å^3$
Z, density (calculated)	4, 0.876 Mg/m^3
absorption coefficient	0.691 mm^{-1}
F(000)	19136
crystal size	0.37 × 0.37 × 0.22 mm^3
θ-range for data collection	3.01−36.35°
index ranges	$-31 \le h \le 36$, $-36 \le k \le 30$, $-23 \le l \le 23$
reflections collected	42551
independent reflections	8238 [R(int) = 0.1111]
observed reflections [$I > 2\sigma(I)$]	4469
completeness to θ = 36.35°	99.9%
max and min transmission	1.0000 and 0.4321
refinement method	full-matrix least-squares on F^2
data/restraints/parameters	8238/82/465
goodness-of-fit on F^2	1.532
final R indices[a] [$I > 2\sigma(I)$]	R_1 = 0.1832, wR_2 = 0.4301
R indices (all data)	R_1 = 0.2270, wR_2 = 0.4755
largest diff peak and hole	0.890 and −0.512 e·$Å^{-3}$

[a] $R_1 = \Sigma||F_o| - |F_c||/\Sigma|F_o|$, $wR_2 = [\Sigma w(|F_o|^2 - |F_c|^2)^2/\Sigma w(|F_o|^2)^2]^{1/2}$.

Determination of Changes in Planar Cell Surface Area (PCSA). The human mesangial cells (HMC) were plated in 20 mm plates, and studies were performed before they reached confluence. Cells were pretreated with the different compounds and then treated successively with AII. The cells were observed under phase contrast with an inverted PFX model TMS-F photomicroscope (magnification, 100×). Photographs of cells were taken at 0 min and after 30 min of AII treatment. Every cell with a sharp margin suitable for the planimetric analysis was considered, and 6−12 cells were analyzed per photograph. PCSA was determined by computer-aided planimetric techniques. Measurements were performed by three different researchers in a blind fashion.

Antioxidant Properties. In these experiments, telmisartan and the copper complex were dissolved in the minimum quantity of DMF in order to avoid precipitations, and then they were added to the aqueous buffer and the substrate solutions. The same quantity of DMF was added to the solutions for the basal state measurements in each case. The concentration of DMF in each test was different but achieved a maximum of 2% in the final reaction mixtures. The antiradical activities of the compounds: the scavenging power of the 1,1-diphenyl-2-picrylhydrazyl radical ($DPPH^{\bullet}$) radical, the total antioxidant activity measured by the 2,2′-Azinobis(3-ethylbenzothiazoline-6-sulfonic acid) diammonium salt ($ABTS^{+\bullet}$) decoloration assay, the inhibition of peroxyl radical, and the sequestering power of superoxide anion were measured in triplicate according to previously reported methods.[16]

Cell Culture. Human lung cancer cell line A549 was obtained from ABAC (Argentinean Cell Bank Association INEVH, Pergamino, Buenos Aires, Argentina). Cells were maintained at 37 °C in a 5%

dx.doi.org/10.1021/ic500483p | Inorg. Chem. XXXX, XXX, XXX−XXX

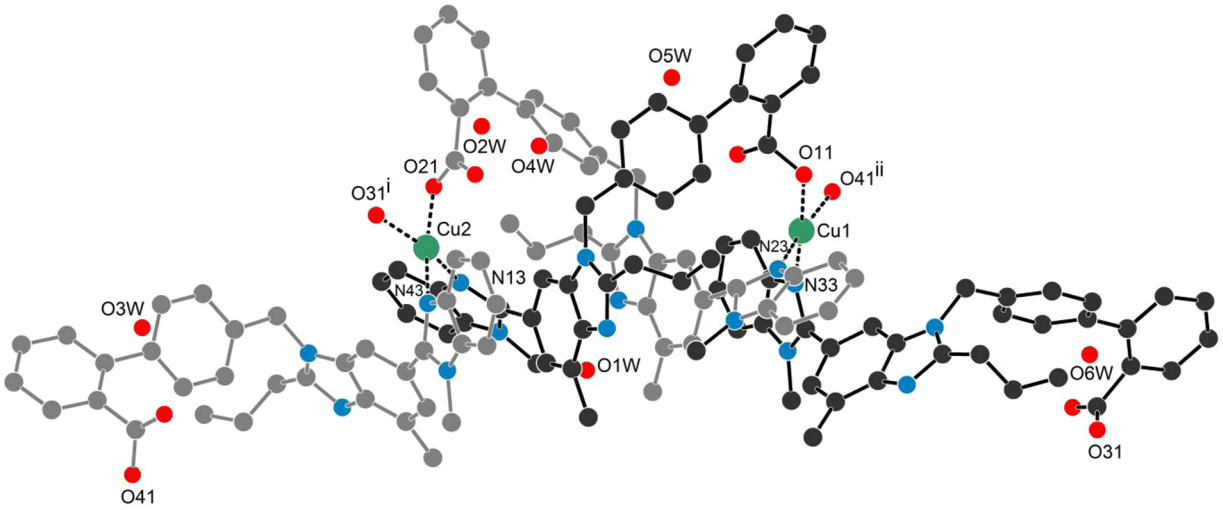

Figure 2. Independent molecular fragment of $[Cu_8Tlm_{16}]\cdot 24H_2O$ complex. For clarity, the H atoms are not included in the drawing and only are labeled the copper ions, the core N_2O_2 bonded-to-copper ligand atoms, and the water molecules. For the same reason, only the shorter Cu−O bonds (in dashed lines) have been included in the drawing. Copper, oxygen, and nitrogen atoms are shown as disks of respectively green, red, and blue color. Crystal symmetry operations: (i) y, $3/2 - x$, z; (ii) $3/2 - y$, x, z.

carbon dioxide atmosphere using the following culture medium: Dulbecco's Modified Eagles medium (DMEM) supplemented with 100 U/mL penicillin, 100 μg/mL streptomycin, and 10% (v/v) fetal bovine serum. When 70−80% confluence was reached, cells were subcultured using TrypLE from Gibco (Gaithersburg, MD, USA), free phosphate buffered saline (PBS) (11 mM KH_2PO_4, 26 mM Na_2HPO_4, 115 mM NaCl, pH 7.4). For experiments, cells were grown in multiwell plates. When cells reached 70% confluence, the monolayers were washed twice with DMEM and then incubated with the different compounds.

Human mesangial cell lines (HMC) were cultured according to previously described procedures.[24] Portions of macroscopically normal cortical tissue were obtained from human kidneys immediately after a nephrectomy was performed because of renal cell carcinoma. Isolated glomeruli were treated with collagenase (Sigma) and plated on plastic culture dishes (Nunc, Kamstrup, Denmark). The identity of the cells was confirmed by previously described morphological and functional criteria.[24] When cells reached confluence, they were subcultured at a ratio of 1−4 in RPMI 1640 supplemented with 10% fetal bovine serum (BioWhittaker, Walkersville, MD). Approval was granted by the Hospital Universitario Príncipe de Asturias Ethics Committee. The use of HMC was performed in accordance with the Declaration of Helsinki.

The prostate cancer cell lines LNCaP (androgen-sensitive), PC-3 (androgen-independent, derived from metastatic site: bone), and DU 145 (androgen-independent, derived from metastatic site: brain) were obtained from the American Type Culture Collection (ATCC, Manassas, VA, USA). The cell lines LNCaP, PC-3, DU 145, and HMC were cultured in RPMI 1640 medium supplemented with 100 U/mL penicillin, 100 μg/mL streptomycin, and 7% or 10% (v/v) fetal bovine serum (FBS) (Invitrogen, Prat de Llobregat, Barcelona, Spain).[25,26]

Cytotoxicity Assays. The compounds were dissolved in DMSO just before the experiment, and a calculated amount of these solutions was added to the growth medium containing cells at a final solvent concentration of 0.5%, which had no discernible effect on cell killing. The growth inhibitory effect toward the cancer A549 cell line was evaluated by means of the crystal violet bioassay. Briefly, 2.0×10^4 cells/well were seeded in 48-well microplates in growth medium (500 μL) and then incubated at 37 °C in a 5% carbon dioxide atmosphere. After 24 h, the medium was removed and replaced with a fresh one containing the compounds to be studied at the appropriate concentration. Triplicate cultures were established for each treatment. After 24 h, each well was treated with crystal violet and washed to remove the excess of dye. The crystal violet taken up by the cells was extracted with the buffer, and the inhibition of cell growth induced by the tested compounds was detected by measuring the absorbance of each well at 540 nm. Mean absorbance for each drug dose was expressed as a percentage of the control untreated well absorbance and plotted versus drug concentration.

For the metabolic activity determinations of the prostate cancer cell lines, the cells were seeded into 24-well plates at a density of 2×10^4 per well. After 48 h, the medium was removed, and the cells were washed with PBS and cultured in RPMI 1640 with 10% FBS containing the compounds to be studied at the appropriate concentration. Triplicate cultures were established for each treatment. After 24 h, the medium was removed and 3-[4,5-dimethylthiazol-2-yl]-2,5-diphenyltetrazolium bromide (MTT) stock solution in PBS was added to the culture (final concentration 0.5 mg/mL) and cells were incubated (2.5 h, 37 °C). Formazan crystals were dissolved in DMSO, and absorbance was measured on a microplate reader (test wavelength 570 nm, reference wavelength 690 nm).[27] At least three independent experiments were performed for each experimental condition in all the biological assays. Results are expressed as mean ± SEM (standard error of the mean). Statistical differences were analyzed using the ANOVA method followed by the test of LSD Fisher (least significant difference).

Flow Cytometric Analysis of Apoptosis. Apoptosis was identified and quantified by flow cytometry with propidium iodide staining. Adherent and floating cells were collected after treatment, NP-40 10% (nonyl phenoxypolyethoxyethanol (Tergitol-type NP-40)) was added, and cells were treated with RNase (1 mg/mL, 30 min, in ice). Cellular DNA was stained with 5 ng/mL propidium iodide (PI) in phosphate-buffered saline, and cells were analyzed on a FACScan flow cytometer (Becton Dickinson, BD Biosciences, San Agustín de Guadalix, Madrid, Spain). Percentages of cells in different cell-cycle phases were calculated from DNA histograms. Cells with sub-G1 DNA content were considered apoptotic.[28]

Antimicrobial Assays. Antibacterial activity was evaluated by the minimum inhibitory concentration (MIC) on five strains of bacteria derived from the American Type Culture Collections (ATCC), namely, *Escherichia coli* (ATCC 35218), *Pseudomonas aeruginosa* (ATCC 27853), *S. aureus* (ATCC 25923), *S. epidermidis* (ATCC 1263), and *Enterococcus faecalis* (ATCC 29212). Antifungal activity was evaluated by the MIC on tree strains of fungus (*Candida parapsilosis* ATCC 22019, *Candida tropicalis*, and *Candida albicans* of clinical isolates). The MICs were determined using the agar dilution method. The cultivation/assay medium for all strains was Mueller

dx.doi.org/10.1021/ic500483p | *Inorg. Chem.* XXXX, XXX, XXX−XXX

Table 2. Selected Bond Lengths [Å] and Angles [°] around Copper(II) Ions in $[Cu_8Tlm_{16}]\cdot 24H_2O$[a]

Cu(1)−N(23)	1.84(1)	O(41)#1−Cu(1)−O(11)	86.9(6)
Cu(1)−N(33)	1.99(1)	N(23)−Cu(1)−N(33)	89.9(5)
Cu(1)−O(11)	1.97(2)	O(41)#1−Cu(1)−N(33)	90.8(5)
Cu(1)−O(41)#1	1.94(1)	O(11)−Cu(1)−N(33)	174.5(6)
Cu(2)−N(13)	2.06(2)	O(21)−Cu(2)−O(31)#2	85.6(5)
Cu(2)−N(43)	1.99(2)	O(21)−Cu(2)−N(43)	167.9(6)
Cu(2)−O(21)	1.97(1)	O(31)#2−Cu(2)−N(43)	93.0(7)
Cu(2)−O(31)#2	1.99(2)	O(21)−Cu(2)−N(13)	90.9(6)
		O(31)#2−Cu(2)−N(13)	161.4(7)
N(23)−Cu(1)−O(41)#1	174.3(5)	N(43)−Cu(2)−N(13)	94.1(7)
N(23)−Cu(1)−O(11)	92.9(6)		

[a]Symmetry transformations used to generate equivalent atoms: (#1) $y, -x + 3/2, z$; (#2) $-y + 3/2, x, z$.

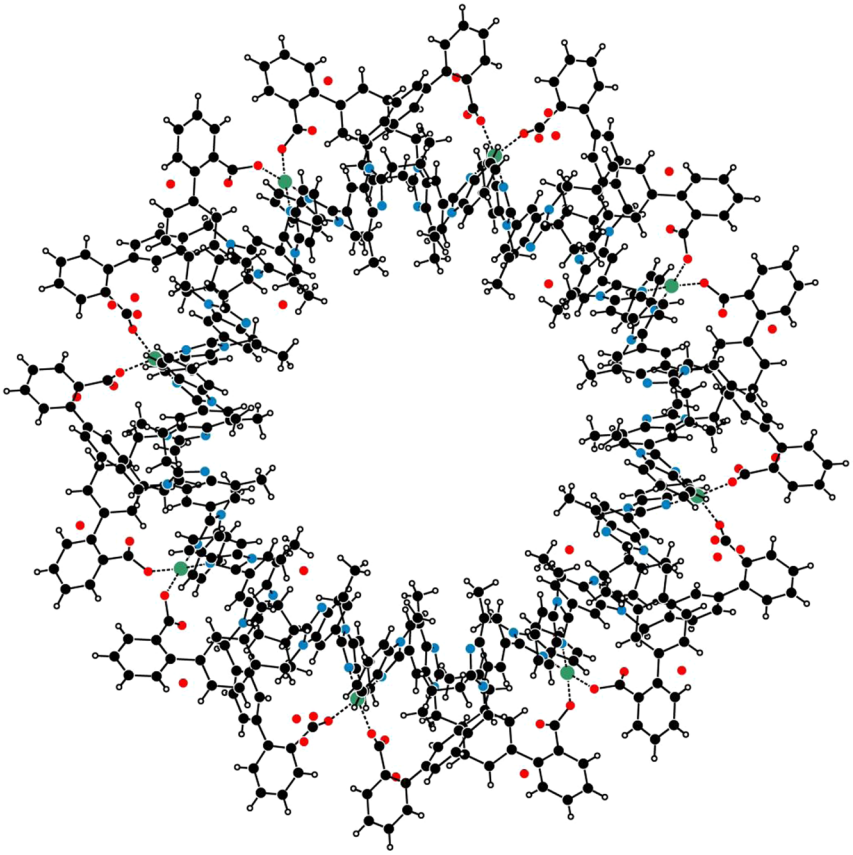

Figure 3. View of the complete $[Cu_8Tlm_{16}]\cdot 24H_2O$ octanuclear Cu(II) complex, obtained from the independent $[Cu_2Tlm_4]\cdot 6H_2O$ fragment depicted in Figure 2 through the crystal C_4 symmetry operations.

Hinton broth or agar.[29,30] The inocula of bacterial strains were prepared from 18 h old broth cultures. A McFarland 0.5 suspension was prepared for each microorganism, and a 1:10 dilution was made prior to inoculation (~10^7 colony forming units (CFU) per milliliter).[31,32] The inocula of fungal strains were adjusted to 0.5 McFarland, and this suspension (~10^8 CFU per milliliter) were directly inoculated without dilution.

For the agar dilution method, aqueous solutions of the metal salt ($CuCl_2\cdot 2H_2O$) were prepared. The ligand and the Cu(II) complex were dissolved in dimethyl sulfoxide. Besides, candesartan (2-ethoxy-1-({4-[2-(2*H*-1,2,3,4-tetrazol-5-yl)phenyl]phenyl}methyl)-1*H*-1,3-benzodiazole-7-carboxylic acid) and its copper(II) complex ($[Cu(Cand)(H_2O)_4]$) were tested for the sake of comparison. All these solutions were sterilized by filtration using membrane filters with pore size 0.22 μm. Serial 2-fold dilutions were prepared from the stock solution in molten Mueller Hinton agar medium and cooled down to 45 °C to obtain the desired final concentrations. Dosage of each chemical started from 2.93 μg mL^{-1} and continued until 1500 μg mL^{-1} (stopping criterion). Then, the inoculums of 2 μL of the microbial suspensions were streaked onto the plates and incubated aerobically at 37 °C for 24 and 48 h for bacteria and fungi, respectively.

Inhibition of microbial growth in the plates containing tested solutions was judged by comparison with growth in blank control plates. The MIC was defined as the lowest dilution of the complex that inhibited the visible growth of the test organism.

RESULTS AND DISCUSSION

Discussion of the Structure. The content of the crystal asymmetric unit ($[Cu_2Tlm_4]\cdot 6H_2O$) is shown in the ORTEP[33] plot of Figure 2, and selected bond distances and angles around the two independent copper atoms are listed in Table 2. The Cu(II) ions are in a distorted bipyramidal environment with a somewhat twisted square basis, cis-coordinated at their basis to

dx.doi.org/10.1021/ic500483p | Inorg. Chem. XXXX, XXX, XXX−XXX

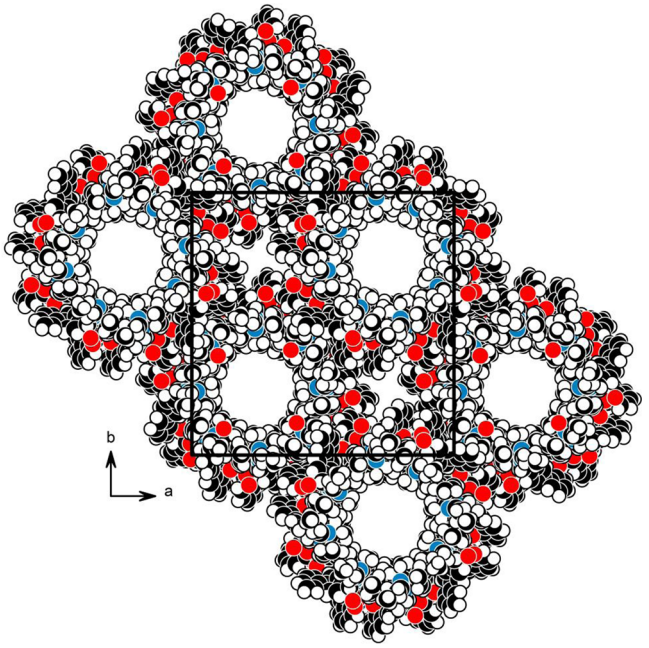

Figure 4. Space-fill crystal packing view of $[Cu_8Tlm_{16}]\cdot 24H_2O$ along the tetragonal *c*-axis showing the nanochannels defined by the toroidal-like shaped $[Cu_8Tlm_{16}]$ complexes. Also shown are the interstitial subnanometer channels along the $\bar{4}$ crystal axis produced by the arrangement of close-packed nanotubes in the lattice.

two carboxylate oxygen atoms [Cu−O distances of 1.97(2) and 1.99(2) Å for Cu1 and 1.97(1) and 1.99(2) Å for Cu2] and to two terminal benzimidazole N atoms [Cu−N distances of 1.84(1) and 1.99(1) Å for Cu1 and 2.06(2) and 1.99(2) Å for Cu2], respectively, belonging to the four different negatively charged telmisartan ligands. The torsion NNOO angles involving the core N_2O_2 ligands at the pyramid basis are 7.6(6)° and 20.9(6)° for Cu1 and Cu2. The bipyramid apexes are occupied by the other carboxylate oxygen atom at strongly distorted positions [Cu−O lengths of 2.81(2) and 2.90(2) Å for Cu1 and 2.61(2) and 2.84(2) Å for Cu2]. The Cu_2Tlm_4 molecular fragment is sited around a crystallographic 4-fold axis (C_4) giving rise to an octanuclear Cu(II) complex (Cu_8Tlm_{16}), as shown in Figure 3. This can be viewed as a macrocyclic ring having a double helical structure with adjacent ligand (L) single turns linked through the copper(II) ions. The helical conformation is afforded by the relative rotational freedom of the charged telmisartan molecule around the σ-bonds linking its groups. In fact, the torsion angle around the phenyl-methylene, the benzoic phenyl−phenyl, and the phenyl−COO bonds shows a maximum variation among the four ligands of 75(3)°, 73(1)°, and 42(2)°, respectively. The torsion angle around the bond linking the benzimidazole groups shows a somewhat smaller variation of 25(3)°. There are eight complete helical turns around the complex with slightly different and alternated pitches defined by neighboring Cu···Cu distances (10.842(4) and 10.472(4) Å). This confers the complex a toroidal-like shape with an average diameter (defined by the distance between two C_2-symmetry related copper atoms) of 27.837(6) Å that leaves a hydrophobic nanohole, lined by benzimidazole methyl groups, of cross dimensions in the range from 15.81(4) to 19.84(4) Å (distances between opposing C_2-related methyl carbons). The Cu_8Tlm_{16} complexes are arranged in the crystal such as to define the inner bonds of channels that extend through the solid along the crystal *c*-axis (see Figure 4). These molecular nanometer tubes, in turn, are close-packed to give rise to smaller interstitial subnanometer channels, lined by benzoic phenyl rings, that runs along the $\bar{4}$ crystallographic axes. The oxygen atoms of the crystallization water molecules are at close contact distances from H-bond acceptors. Four of them are close to weakly bonded-to-metal carboxylate oxygen atoms [Ow···O distances in the range from 2.86(2) to 3.00(3) Å], a fifth one is at a distance of 2.90(2) Å from a benzimidazole N atom, and the sixth one is in close contact with other water oxygen atom [d(Ow···Ow) = 2.95(5) Å].

Vibrational spectra. The main characteristic experimental vibrations of telmisartan and the copper complex obtained from FTIR and Raman spectra are shown in Table 3. The vibrational assignments were performed according to the literature data.[34−36] The spectra of telmisartan has also been compared with those of irbesartan,[37] candesartan, and valsartan[38] and with previous experimental vibrational assignments performed for valsartan and its copper coordination complex.[16] Bands located at 4000−2000 cm^{-1} spectral range were assigned to O−H and C−H stretching vibrations. The broad FTIR band of CuTlm at 3389 cm^{-1} assigned to O−H stretching modes of water molecules masked the observation of the changes in this region.

The strong band of free telmisartan at 1696 cm^{-1} (s, FTIR) associated with the C═O stretching of the carboxylic acid moiety disappeared in the copper complex. New bands assigned to both antisymmetric and symmetric stretching modes of the carboxylate group generated by coordination of the carboxylic acid moiety were observed at 1587 cm^{-1} (s, FTIR) and 1395 cm^{-1} (vs, FTIR) and 1396 cm^{-1} (m, Raman), respectively. The difference between the antisymmetric and the symmetric frequencies Δ = 192 cm^{-1} suggested a monodentate coordination mode of the carboxylate group to the metal center,[34] as uncovered by the X-ray crystal structure. Typical bands of benzimidazol (Bz) in the 1600−1400 cm^{-1} range were found in the same region than the characteristic bands of the biphenyl group.[39,40] These modes are coupled with CH_3 and CH_2 wagging, torsion and bending deformation modes. The disappearance of the characteristic bands of Bz at 1481 cm^{-1} (s) and 1468 cm^{-1} (s) in the Raman spectrum of telmisartan and the appearance of a new band at 1448 cm^{-1} (s) in the Raman spectrum of CuTlm indicated structural changes in Bz rings due to a possible interaction with the copper(II) ion with the N moiety of Bz, a fact confirmed by the X-ray study. The bands with a strong/medium (FTIR/Raman) intensities located at 1297 cm^{-1} with components of COH bending[41,42] and CN (Bz) stretching modes of Tlm reduced their intensities upon complexation. Similar changes were observed for the vibrational modes involving those groups (stretching C−O and C−N Bz in the 1234−1125 cm^{-1} range) indicating a metal−ligand interaction. To conclude, the observed shifts of the CN Bz bands and the disappearance of the vibrational modes involved with the carboxylic group would suggest that the binding of the metal with Tlm takes place through these functional groups, as proven by the structural X-ray results.

Electron Spin Resonance Spectra. The X-band EPR powder spectra of $[Cu_8(Tlm)_{16}]\cdot 24H_2O$ has been measured at room temperature (Figure 5, solid line). The anisotropic EPR signal of the polycrystalline sample shows a four-line hyperfine splitting pattern due to the coupling of the unpaired electron and the ^{63}Cu nucleus (I = 3/2). Spectral simulation of the EPR signal is displayed in Figure 5 (dashed line) and proved that the complex exhibits a monomeric type signal, having axial symmetry with sin Hamiltonian parameters of $g_{\|}$ = 2.28, $g_{\perp}$ =

dx.doi.org/10.1021/ic500483p | Inorg. Chem. XXXX, XXX, XXX−XXX

Table 3. Frequency (in cm^{-1}) and Proposed Vibrational Mode Assignment of Bands for the FTIR and Raman Spectra of Telmisartan and Its Copper(II) Complex[a]

	FTIR		Raman	
assignment	CuTlm	Tlm	CuTlm	Tlm
ν O−H		3403 (w)		
ν O−H (H_2O)	3389 (br,m)			
ν C−H_{arom}	3221 (m)			
ν $CH_{arom\ ip}$	3055 (w)	3059 (w)	3058 (m)	3063 (m)
ν $CH_{arom\ op}$	3026 (w)	3033 (w)		
ν CH_{as} CH_3	2961 (m)	2959 (m)	2977 (w)	2959 (w)
ν CH_{as} CH_2, CH_3	2930 (m)	2928 (m)	2945 (w)	2926 (w)
ν CH_s CH_3	2871 (m)	2870 (w)	2916 (m)	2896 (w)
ν C═O (COOH)	1706 (w)	1696 (s)		
ν C═C + ν CN_{Bz}		1613 (w)	1614 (vs)	1613 (vs)
	1602 (s)	1600 (w)	1595 (m)	1600 (m)
ν_{as} COO^-	1587 (s)			
benzimidazole- biphenyl modes (see text)	1572 (m)	1560 (vw)		
	1558 (m)			
	1534 (m)	1522 (w)	1528 (vs)	1523 (vs)
	1516 (m)	1517 (sh,m)		
	1507 (m)			
	1480 (s)	1479 (s)		1481 (sh,s)
	1455 (sh,vs)	1456 (vs)	1448 (s)	1468 (s)
	1445 (vs)	1444 (s)	1439 (m)	1435 (m)
	1409 (s)	1413 (s)		1424 (sh,m)
ν_s COO^-	1395 (vs)		1396 (m)	
δ_{ip} CCH + ν C−$C_{biphenyl}$	1382 (vs)	1383 (m)	1357 (w)	1386 (w)
				1360 (w)
ω CH_2 + ρ CH_2	1338 (s)	1332 (s)	1326 (w)	1339 (w)
δ COH + δ CCH		1323 (m)		
		1305 (s)		
δ COH + δ CCH + τ CH_2 + ν C−C_{bz}+ ν CN_{bz}		1297 (s)	1296 (w)	1297 (m)
	1277 (m)	1267 (vs)	1277 (m)	1277 (m)
	1245 (w)	1246 (s)	1247 (m)	1250 (m)
ν C−O (COH) + δ CCH_{arom}	1234 (w)	1230 (s)		1228 (w)
$\delta_{ip\ arom}$ CCH + ρ CH_2 + ω CH_2 + ν CN_{bz} CNBz	1130 (vw)	1129 (m)	1125 (sh,w)	1129 (m)
	1092 (w)	1089 (w)	1101 (m)	1101 (m)

[a]Abbreviations: vs, very strong; s, strong; m, medium; w, weak; vw: very weak; sh, shoulder. ν, stretching; δ, bending; ω, wagging; τ, twisting; ρ rocking; s, symmetric; as, antisymmetric; arom, aromatic; op, out of plane; ip, in plane; bz, benzimidazole.

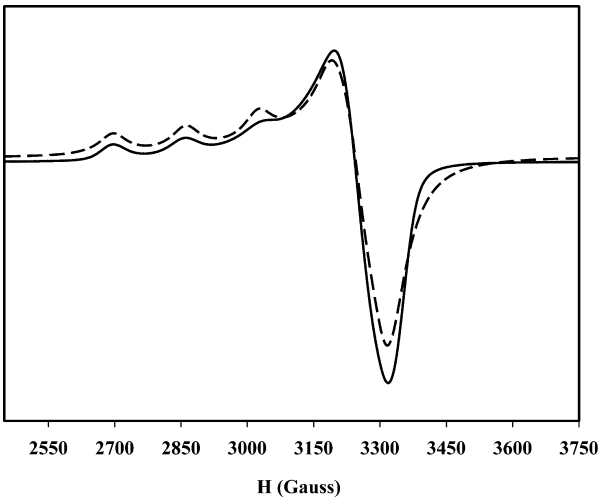

Figure 5. X-band EPR powder spectra at 293 K of the complex $[Cu_8Tlm_{16}]\cdot 24H_2O$ (solid line) and simulated spectrum (dashed line) with WINEPR SimFonia program.

2.061, and $A_{\parallel} = 175 \times 10^{-4}$ cm^{-1}, $A_{\perp} = 10 \times 10^{-4}$ cm^{-1}, typical of elongated octahedral or square planar Cu(II) complexes, as found by the crystallographic study, having metal $d_{x^2-y^2}$ ground state.[43]

The value of the parallel component of the hyperfine coupling constant is comparable to that found in Cu(II) complexes with chromophores containing nitrogen and oxygen atoms in the coordination sphere of the metal center.[44−46] This agrees with the CuO_2N_2 core of the somewhat twisted square planar geometry revealed by X-ray diffraction. Concerning the possibility of magnetic coupling between neighboring Cu(II) ions, it turns out that for axial symmetry the ratio of g-values, namely, $G = (g_{\parallel} - 2)/(g_{\perp} - 2)$, provides an estimation for the magnitude of copper−copper exchange interaction. According to Hathaway[43] a G value less than 4 indicates a considerable exchange interaction in the solid complexes, while a higher value indicates that the magnetic interaction is negligible. For the CuTlm complex, the calculated G value equal to 4.59, hence suggesting that there is no interaction between the copper centers. This magnetic result is substantiated by the X-ray structural one showing that neighboring Cu(II) ions are too far apart from each other (in about 10.5 A) for significant Cu···

dx.doi.org/10.1021/ic500483p | Inorg. Chem. XXXX, XXX, XXX−XXX

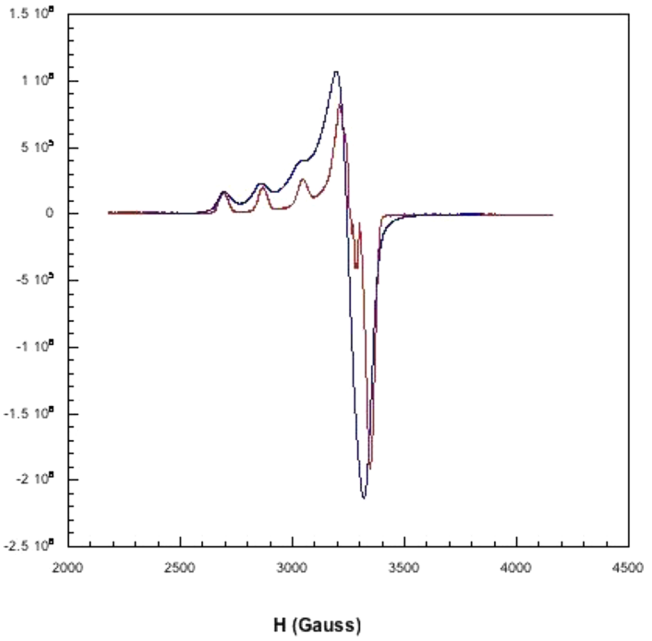

Figure 6. Blue: X-band EPR powder spectra at 293 K of the complex $[Cu_8Tlm_{16}]\cdot 24H_2O$; red: EPR spectrum in DMF (100 μM) at 140 K.

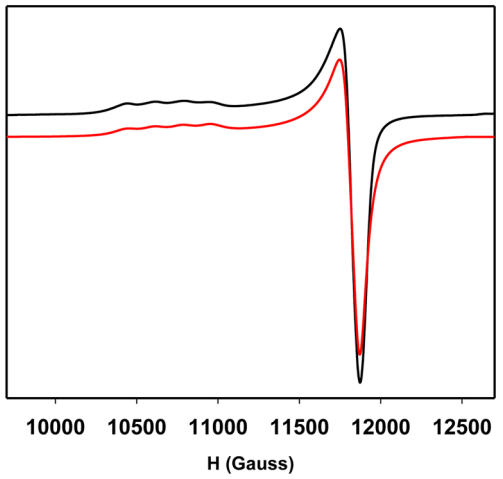

Figure 7. Q-band EPR powder spectra at 293 K of the complex $[Cu_8Tlm_{16}]\cdot 24H_2O$ (black line) and simulated spectrum (red line) with WINEPR SimFonia program.

Cu direct exchange to take place and linked through the telmisartan molecule too extended an electronic pathway for appreciable superexchange to take place.

To evaluate the nature of the species formed upon dissolution of the $[Cu_8Tlm_{16}]\cdot 24H_2O$ complex, EPR spectrum in DMF (100 μM) at 140 K was performed and compared with the solid-state one. From Figure 6, it can be seen that when the fields are normalized, the powder (blue) and the solution DMF spectra (red) overlap reasonably well. From the spectral simulation of the solution spectrum, the spin Hamiltonian parameters of $g_{\parallel} = 2.27$, $g_{\perp} = 2.051$, and $A_{\parallel} = 188.5 \times 10^{-4}$ cm^{-1}, $A_{\perp} = 27 \times 10^{-4}$ cm^{-1} have been calculated and are again typical of elongated octahedral or square planar Cu(II) complexes with a metal $d_{x^2-y^2}$ ground state. Taking into account the EPR parameters and the Blumberg–Peisach approach[47] the $f = g_{\parallel}/A_{\parallel}$ (cm^{-1}) value (120.4) is indicative of square planar environments. This result is consistent with

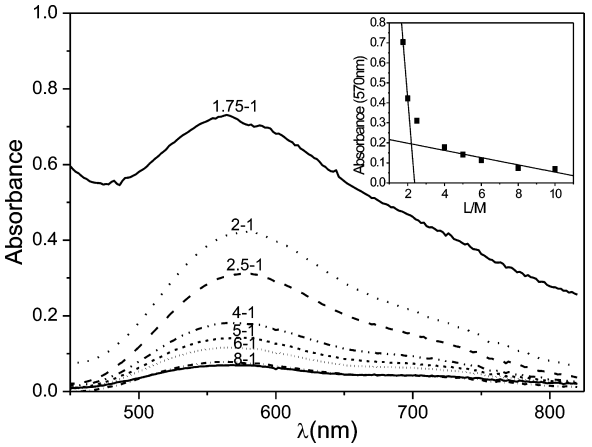

Figure 8. UV–vis spectra of telmisartan (6.25×10^{-3} M) with the addition of $CuCl_2\cdot 2H_2O$ in ligand-to-metal ratios (L/M) from 10.00 to 1.75 (pH 7) Inset: Spectrophotometric determination of CuTlm complex stoichiometry at 580 nm by the molar ratio method.

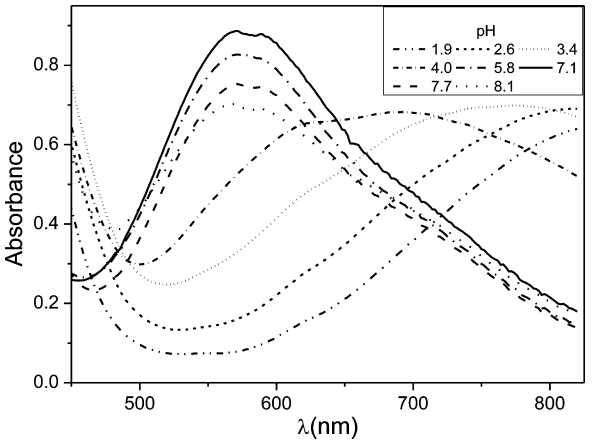

Figure 9. Electronic absorption spectra of $CuCl_2\cdot 2H_2O$ (6.25×10^{-3} M) and telmisartan (1.25×10^{-2} M), ethanolic solutions, for different pH values.

Table 4. Percentage of the Planar Cell Surface Area (PCSA)[a]

compound	% PCSA (mean ± SEM)
CT	100 ± 0.2
AII	81.3 ± 2.3[b]
$CuCl_2\cdot 2H_2O$	87.9 ± 0.04
telmisartan	90.6 ± 0.6[c]
CuTlm	91.3 ± 1.2[c]

[a]CT, basal conditions. Angiotensin II (AII) (10^{-6} M) was added after a previous incubation of the cells with each compound (10^{-8} M) during 15 min. The results are the mean ± SEM from seven independent experiments. [b]Significant differences versus basal $p < 0.05$. [c]Significant differences versus AII $p < 0.05$.

the structure determined by X-ray measurements. Moreover, the Hamiltonian parameters are in concordance with CuO_2N_2 equatorial ligand environment.[48,49]

In addition, the room temperature solid-state EPR spectrum at Q-band was also analyzed (Figure 7), and the calculated spin Hamiltonian parameters, $g_{\parallel} = 2.2765$, $g_{\perp} = 2.058$ and $A_{\parallel} = 185 \times 10^{-4}$ cm^{-1}, $A_{\perp} = 20 \times 10^{-4}$ cm^{-1}, are very close to those obtained in DMF. In conclusion, these EPR results suggest that

dx.doi.org/10.1021/ic500483p | Inorg. Chem. XXXX, XXX, XXX–XXX

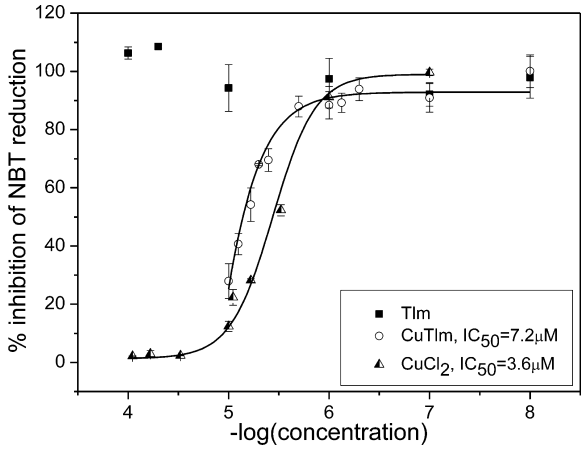

Figure 10. Effects of copper(II), telmisartan (Tlm), and their coordination complex (CuTlm) on reduction of nitroblue tetrazolium by nonenzymatically generated superoxide (phenazine methosulfate and reduced nicotinamide adenine dinucleotide system).

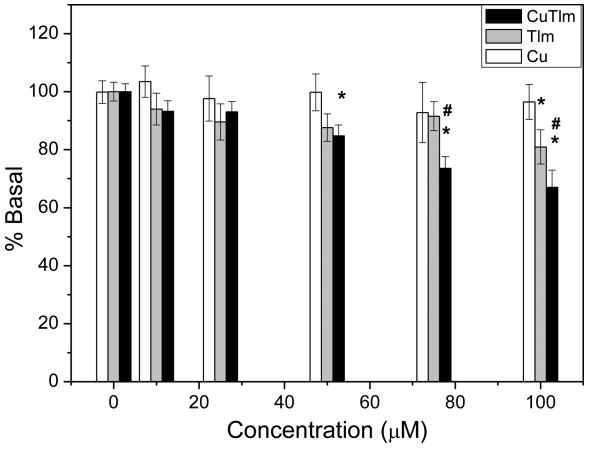

Figure 11. Effects of copper(II), telmisartan (Tlm), and their coordination complex (CuTlm) on human lung cancer cell line A549 viability evaluated by the crystal violet method. Cells were incubated in serum-free DMEM alone (control) or with different concentrations of the compounds at 37 °C for 24 h. The results are expressed as the percentage of the basal level and represent the mean ± SEM (n = 18). *Significant differences versus basal $p < 0.05$. #Significant differences at the same concentration between CuTlm and both Tlm and Cu, $p < 0.05$.

the molecule is not substantially modified and basically retains its solid-state structure in DMF solution.

In summary, the proposed structure of the microcrystalline CuTlm powder considering the stoichiometry of the compound (elemental analysis), the presence of three water molecules (thermogravimetric analysis (TGA) determinations) per copper atom, and the spectroscopic characterization of the solid complex: square planar CuO_2N_2 environment with no interaction between copper centers (EPR measurements) and interaction with carboxylate (monodentate) and N (Bz) moieties of the ligand (FTIR, Raman observations) closely agree with the single crystal X-ray structural determination. Furthermore, the diffuse reflectance and the electronic UV−vis spectra of the powder and the crystals of CuTlm showed the same pattern (data not shown).

Spectrophotometric Titrations and Stability Studies. With the aim of identifying the solution species present at the pH value of the preparative, spectrophotometric titrations were achieved. A fixed concentration of telmisartan (6.25 mM) was maintained while different copper(II) concentrations were added fixing the final pH value to 7 for each metal-to-ligand ratio by the addition of 1 M NaOH. The measured UV−visible spectra are shown in Figure 8. All the spectra showed two electronic absorption bands located at 570 and 720 nm (sh). The small difference in band position with the diffuse reflectance spectrum may be due to solvatochromic effects. By the molar ratio method, it can be determined that the stoichiometry of the complex formed in solution (2:1 L:M) is in agreement with that determined for the solid compound (Figure 8, inset).

Complex formation was also observed at different pH values with M:L ratios 2:1, ethanolic solutions (Figure 9). The typical electronic spectrum of copper(II) at acidic pH values (λ_m > 820 nm) was an indication that the interaction with the ligand was negligible. At higher pH values (pH 6), a hypsochromic shift was produced as a consequence of complex formation, and the new bands were located at 570 and 720 nm (sh). These features remained unaltered up to pH values near 8. At pH > 8 a precipitate was formed probably because of the decomposition of the complex and the subsequent copper(II) hydroxide and/or oxide formation.

The stability studies were performed with the same solvent used for the biological studies (DMF). It was observed that the complex was stable in DMF, and after 5 h of dissolution the absorbance of the complex diminished about 8% (data not shown). On the other hand, the stability of the complex under biological conditions was determined using 40 μM CuTlm in 0.5% DMSO in PBS. In this case, the complex is stable during the first 1 h and then the absorbance diminished 15% in 3 h. The time of manipulation of the complex before the addition to the cells (15 min) allowed us to determine that the complex remained stable in the dissolution with DMF and under biologically relevant conditions.

Reduction of Planar Cell Surface Area in Human Mesangial Cells. We have previously determined that candesartan inhibits the AII-induced PCSA reduction in HMC (inhibition of the contractile response to AII) (PCSA = 86.3%) and that this effect improves upon copper complexation (PCSA = 100.8%). This is illustrated in Table 4 where it is compared the effect due to telmisartan and CuTlm. In this case, it is demonstrated that the antihypertensive effect of telmisartan (higher expansive activity on the surface area of HMC) is better than that for candesartan and it is preserved upon complexation.

Docking model studies for the interaction between commonly used ARBs and AT1 receptor were previously performed in order to determine which of the molecular interactions of telmisartan with the AT1 receptor could explain the strongest blood pressure lowering activity of telmisartan. It was demonstrated that telmisartan has a unique binding mode to the AT1 receptor, and it was found to be a sole ARB that could entirely fill the binding pocket of AT1 receptor and restrict its conformation via its distal benzimidazole portion. This unique portion could explain the highest molecular lipophilicity, the greatest volume distribution, and the strongest binding affinity of telmisartan to AT1 receptor. Furthermore, telmisartan was found to strongly bind to the AT1 receptor through the unique "'delta lock"' structure. This unique structure is involved in its strongest binding affinity to angiotensin II type 1 receptor, and then it may be superior

dx.doi.org/10.1021/ic500483p | Inorg. Chem. XXXX, XXX, XXX−XXX

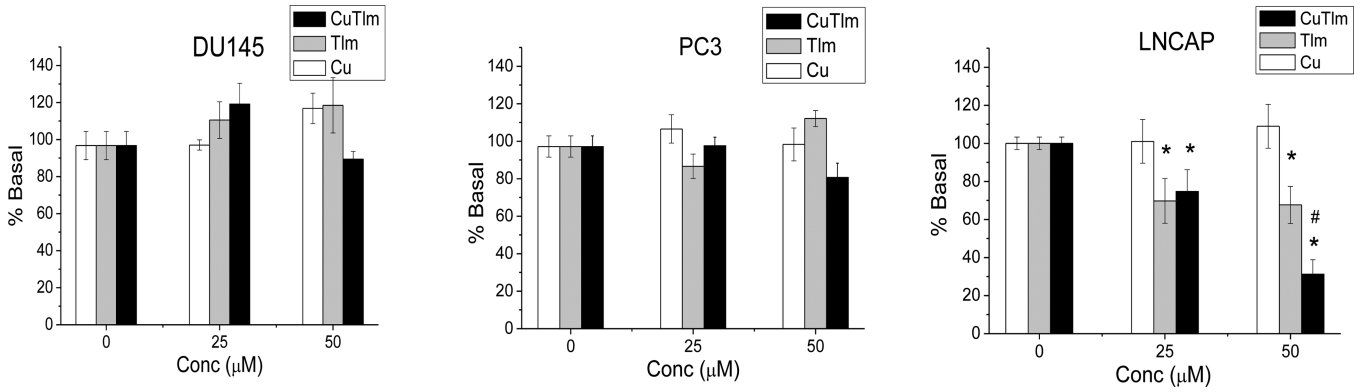

Figure 12. Effects of copper(II), telmisartan (Tlm), and their coordination complex (CuTlm) on human prostate cancer cell lines LNCaP, PC3, and DU 145 viability determined by the MTT assay. Cells were incubated in RPMI with 10% FBS (control) or with different concentrations of the compounds at 37 °C for 24 h. The results are expressed as the percentage of the basal level and represent the mean ± SEM (n = 9). *Significant differences versus basal $p < 0.05$. #Significant differences at the same concentration between CuTlm and both Tlm and Cu, $p < 0.05$.

to other ARBs in arresting cardiovascular disease in patients with hypertension.[50] The interaction of the carboxylate and N (Bz) moieties of the ligand to copper(II) in the complex may induce conformational changes that do not improve enough the pocket binding ability of telmisartan, this being a possible reason for the similar behavior of both compounds. On the contrary, it was demonstrated that in the docking of candesartan into the AT1 receptor model the anionic tetrazole ring does not appear to interact with any residue and that the conformational changes upon coordination probably fitted most of the binding pocket of the AT1 receptor, hence enhancing the properties as AII receptor blocker.[16]

Antioxidant Activities. Hypertension is associated with increased vascular oxidative stress; however, there is still a debate whether oxidative stress initiates the development of hypertension, or if it is a consequence of the vascular damage observed in hypertension. The possible mechanisms by which oxidative stress may cause hypertension are the quenching of the vasodilator nitric oxide, the generation of vasoconstrictor lipid peroxidation products, the damage inflicted to endothelial cells, the damage to vascular smooth muscle cells, or the increase in intracellular free calcium concentration. The hypothesis that increased blood pressure is associated with increased oxidative stress in animals is not supported in human studies. Treatments with supplement antioxidants have failed to show benefits in lowering blood pressure. It is noteworthy that lowering blood pressure with antihypertensive medications is associated with reduced oxidative stress. Therefore, it seems that oxygen stress is not the cause, but rather a consequence, of hypertension.[51]

In general, sartans are not effective free radical scavengers. We have previously determined that candesartan and its copper complex are not good antioxidant agents against $ROO^{\bullet}$, $DPPH^{\bullet}$, and $ABTS^{+\bullet}$. However, the poor antioxidant capacity of candesartan against superoxide anion was improved by complexation $IC_{50} = 6.8 \times 10^{-6}$ M.[16] While the copper complex of losartan ($IC_{50} = 72.1 \times 10^{-6}$ M) shows a moderate superoxide dismutase mimetic activity, the parent sartan does not display antioxidant capacity.[14] Telmisartan and its copper complex did not show antioxidant activities against peroxyl, $DPPH^{\bullet}$, and $ABTS^{+\bullet}$ radicals (data not shown). The SOD mimetic assay (Figure 10) showed that telmisartan does not behave as a superoxide anion scavenger agent, while its copper complex actually improved the effect and proved to be an effective scavenger of the superoxide anion. The concentration of the complex required to attain 50% inhibition of the reduction of the substrate (50% basal conditions) is 7.2×10^{-6} M.

Among reactive oxygen species (ROS), superoxide anion ($O_2^{\bullet -}$) plays important roles in the pathogenesis of many cardiovascular diseases, including hypertension and atherosclerosis. In addition, there is a large body of evidence showing that the exogenous enzyme superoxide dismutase, SOD, plays a critical role in inhibiting oxidative inactivation of nitric oxide (NO) thereby preventing peroxynitrite formation ($ONOO^-$) and endothelial and mitochondrial dysfunction.[52] In a previous report, it was determined that SODs are localized at distinct compartments (cytosol (for SOD1), mitochondria (for SOD2), and extracellular matrix (for SOD3)), participating in compartmentalized redox signaling to regulate many vascular functions. Agents such as vitamin E and vitamin C are not targeted to sites of ROS generation that are most important in pathological conditions. This fact may be a possible explanation of why clinical trials have found no benefits of vitamin E supplementation on cardiovascular disease risk.

Taking into account that telmisartan is not a SOD mimetic compound but it is a good antihypertensive agent and that the new complex CuTlm behaved as a good antioxidant agent and as an antihypertensive compound as good as its parent sartan, the new complex could be used not only against the hypertension disease but also against $O_2^{\bullet -}$ species generated as a consequence of the oxidative stress induced by hypertension.

Cytotoxicity Assays. Copper compounds were particularly effective as anticancer agents confirming the hypothesis that copper conjugation enhanced the biological activity of active ligands. Copper species possess a broader spectrum of activity and a lower toxicity than platinum drugs exerting different mechanism of action.[53] Examples include multiple metal environments. A moderate cytotoxicity against A549 cancer cells (IC_{50} 10−50 μM) was found for CuO_4 coordination spheres. Copper species with a CuN_2O_2 square-planar environment have been shown to possess high SOD mimetic activity and were approximately seven times more active than cisplatin against A549, LNCaP, and DU145 cancer cells.[54] A series of CuN_2Cl_2 complexes had significant cytotoxic activity against the PC3 cancer cell line, and another series with $CuN_2Cl(H_2O)_n$ coordination sphere displayed cytotoxicity

dx.doi.org/10.1021/ic500483p | Inorg. Chem. XXXX, XXX, XXX−XXX

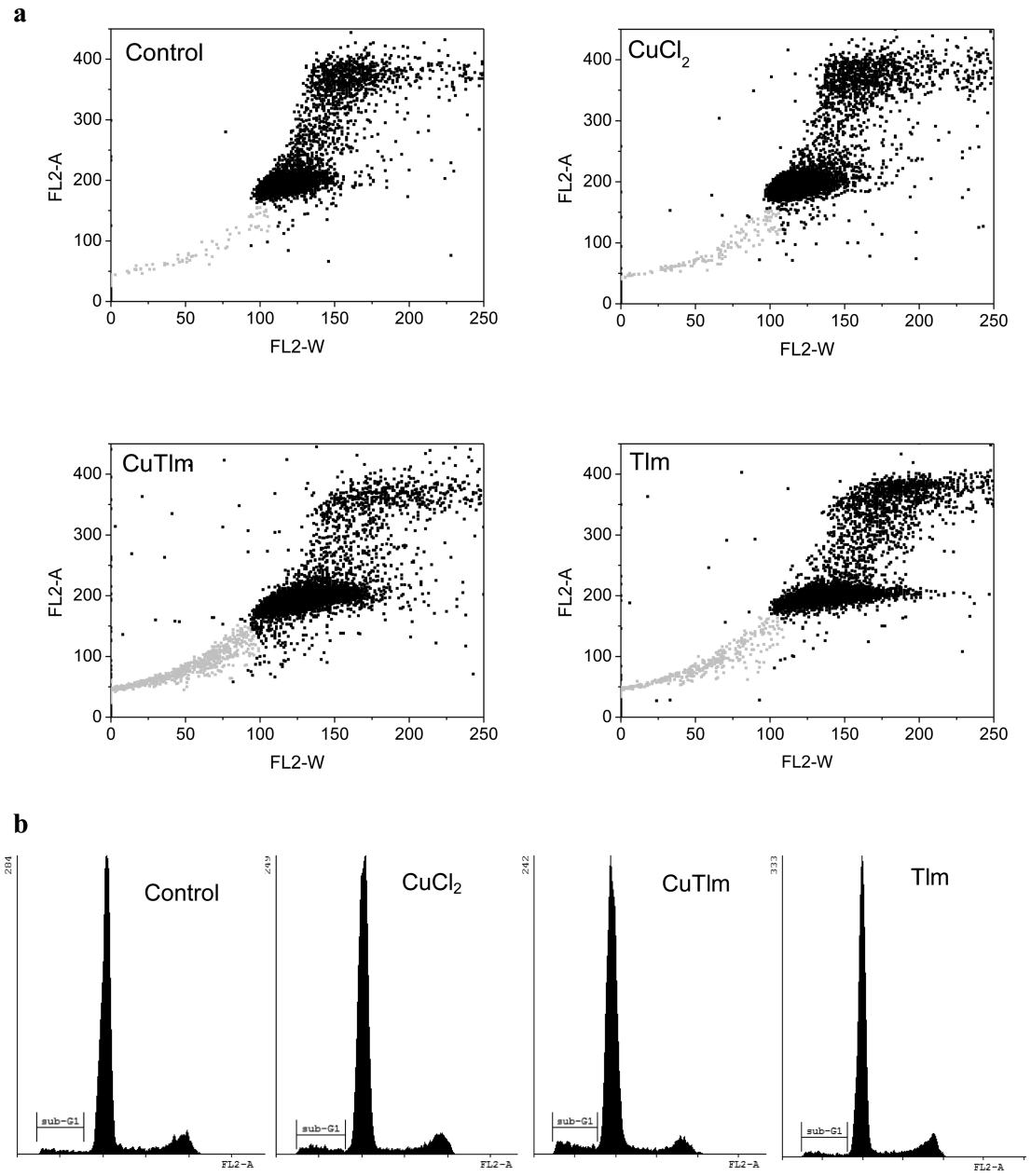

Figure 13. Apoptosis was analyzed by flow cytometry. LNCaP cells were stained with propidium iodide after 24 h of treatment with 50 mM of CuTlm, Tlm, and $CuCl_2$. A total of 10000 events were collected. (a) Dot plot of FL2-A/FL2-W. Sub-G1 phases for each treatment are shown in gray. (b) Histogram with low-molecular fragments of DNA excluded. Sub-G1 hypodiploid cell population was marked between bars.

against A549 cell line.[53] We have previously determined the harmless effect of losartan and valsartan against osteosarcoma UMR106 cell lines[14,15] up to 100 μM concentrations and showed that their copper complexes exhibited inhibitory effects on cellular proliferation (ca. 60% and 40%, respectively), behaving as deleterious agents. It can be seen that complexation of the antihypertensive drugs with the biometal copper modulates their biological effects.

The complex CuTlm, the corresponding free ligand, and $CuCl_2$ salt were examined for their cytotoxic properties against human lung cancer A549 cells (Figure 11). These data showed that telmisartan and copper(II) proved to be ineffective in the tumor cell line up to 100 μM concentrations. On the contrary, CuTlm showed some growth inhibitory potency toward tumor cells (ca. 30% of inhibition of cellular proliferation at 100 μM).

We also evaluated the viability effects of the CuTlm complex, the corresponding free ligand, and the copper salt on three prostate cancer cell lines (LNCaP, PC-3, and DU 145) by the MTT assay. As shown in Figure 12, we observed a greater LNCaP (androgen-sensitive) cell viability decrease when they were incubated with CuTlm for 24 h (ca. 70% of inhibition of cellular viability at 50 μM). However, the PC-3 and DU 145 (androgen-independent) cell viability remain practically unchanged in all treatment conditions (Figure 12).

The MTT assays were also used to demonstrate that human mesangial cells were not damaged by the different compounds under the experimental conditions of the reduction of PCSA tests (incubation time and concentrations). Cells treated with AII, $CuCl_2$, Tlm, CuTlm, $CuCl_2$ + AII, Tlm + AII, and CuTlm + AII did not show significant differences in cell survival with respect to the basal state (data not shown).

dx.doi.org/10.1021/ic500483p | Inorg. Chem. XXXX, XXX, XXX−XXX

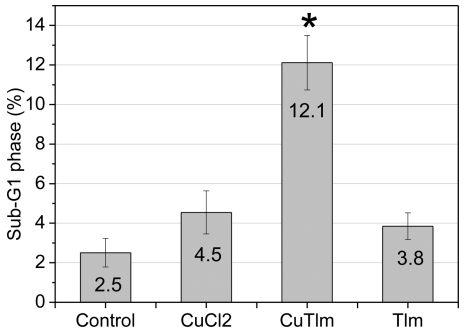

Figure 14. Percentage of sub-G1 hypodiploid cell population on exposure of LNCaP cells to 50 μM $CuCl_2$, CuTlm, Tlm. Values are expressed as the mean ± standard error of at least three independent experiments. *Significant differences versus control $p < 0.05$.

According to the cytotoxic results, LNCaP prostate cancer cells exhibited the highest sensitivity to the complex. Thus, this cell line was used for further investigation of the underlying mechanisms accounting for the cytotoxic action of the complex. To further analyze the mechanism by which the CuTlm diminishs the cell viability on the LNCaP cell line, the cell cycle phase distribution was analyzed by flow cytometry with PI staining. We analyzed the sub-G1 hypodiploid cell population by flow cytometry in cells initially cultured in growth medium for 24 h and then incubated with 50 μM CuTlm complex and the corresponding free ligand and metal for 24 h. By plotting the pulse width (FL2-W) versus the pulse area (FL2-A) in a dot plot graph, the sub-G1 hypodiploid population can be observed. In Figure 13a, a marked increment of this population for CuTlm in comparison with the control is shown. The histograms in Figure 13b also display this increment, but, in this case, small fragments of DNA belonging to necrotic cells were excluded. The gated sub-G1 hypodiploid cell population suggested an increase in apoptosis in comparison with control. As shown in Figure 14, treatment of LNCaP cells with 50 μM CuTlm caused a significant increase of 9.6% at sub-G1 phase with respect to control, while $CuCl_2$ and Tlm produced only a nonsignificant increase of 2.0 and 1.3%, respectively. Altogether, these data indicate that the CuTlm complex was capable of inducing a cell viability decrease in the prostate cancer cell line androgen-dependent, through an apoptotic mechanism, whereas it was unable to modulate the cell viability in the androgen independent cells lines.

Antimicrobial Assays. Taking account that some heart diseases are caused by microbial agents (infective endocarditis by *S. aureus*), the combination of an antimicrobial with an antihypertensive drug could be a useful methodology to develop new therapeutic agents.[12] Considering the knowledge that Cu exerts antibacterial properties, we have designed the new coordination complex CuTlm. The results of the antimicrobial activity assays are given in Table 5. The antimicrobial capacity of commercial tablets of losartan and telmisartan were previously tested, and it was found that the compounds had no effect on *E. coli*, *P. aeruginosa*, and *C. albicans*. However, some effects of the drugs were reported against *S. aureus* (ATCC 6538P) with MIC values of 50×10^3 and 2×10^3 μg mL^{-1}, respectively.[55] We herein report the activity of the pure drug (not commercial tablets) and in the *S. aureus* strain ATCC 25923. Candesartan and its copper complex (CuCand) were also measured for comparative purposes. *In vitro* measurements of antimicrobial activities with MIC values greater than 1000 μg mL^{-1} are considered with no relevance from a clinical perspective.[56] In this context, the antimicrobial activity of the metal against all strains of *Candida*, candesartan and CuCand against all tested strains are considered insignificant. The metal shows antibacterial activity and the antimicrobial effect of telmisartan against *E. faecalis*, *S. aureus*, *S. epidermidis*, *C. albicans*, and *C. parapsilosis* has been determined (see Table 5).[57] The complex CuTlm shows the same antimicrobial activity as that of the free ligand telmisartan against *S. epidermidis*, *C. albicans*, and *C. parapsilosis*, and a somehow less antimicrobial activity than telmisartan against *E. faecalis* and *S. aureus*.

The antimicrobial mechanisms of sartans on microbial pathogens are scarcely described in literature. Some studies suggest that some new ARBs might also directly affect bacterial pathogens that express actively ATII angiotensin-binding sites.[58] These atypical receptors were identified on one species of Mycoplasma (*Mycoplasma hyorhynis*) and one species of Acholeplasma (*Acholeplasma laidlawii*).[59] Losartan (the earliest of the ARBs) does not stop ATII from binding at the microbial angiotensin receptors. Candesartan, irbesartan, and olmesartan medoxomil offer widely different blockade effectiveness on receptors of prokaryotic cells. Therefore, if an ARB is able to inhibit the supply of ATII, thus blocking microbe ability to protect itself from destruction by phagocytosis, then it could be classed as an antimicrobial agent.[55] We herein have determined that telmisartan and CuTlm displayed antimicrobial effects against some strains, mainly against *S. aureus* in which they exhibited a higher potency than that of the copper's intrinsic antimicrobial activity.

CONCLUSION

A copper(II) complex with the antihypertensive drug telmisartan was synthesized and characterized by elemental

Table 5. Minimum Inhibitory Concentration (MIC) of the Metal $CuCl_2 \cdot 2H_2O$, the Free Ligands (Candesartan and Telmisartan), and Their Copper(II) Complexes for the Reference Strains, in μg mL^{-1}

	$CuCl_2 \cdot 2H_2O$[a]	candesartan	telmisartan	CuCand	CuTlm
E. coli	375	>1500	>1500	>1500	>1500
P. aeruginosa	375	>1500	>1500	>1500	1500
E. faecalis	375	>1500	750	>1500	1500
S. aureus	375	>1500	94	>1500	188
S. epidermidis	375	>1500	750	>1500	750
C. albicans	>1500	1500	750	1500	750
C. tropicalis	>1500	>1500	1500	1500	1500
C. parapsilosis	>1500	>1500	750	>1500	750

[a]Ref 54.

dx.doi.org/10.1021/ic500483p | Inorg. Chem. XXXX, XXX, XXX−XXX

analysis and electronic, vibrational, and EPR spectroscopies and by structural X-ray diffraction methods. The elemental analysis suggested that the stoichiometry of the complex is 2:1 ligand-to-metal, and the spectral studies indicated that the complexation to the metal ion takes place through nitrogen and oxygen atoms of each ligand. The structure and the coordination mode of the ligand to the metal were established by X-ray crystallography. The octanuclear complexes define the inner bond of hydrophobic channels forming molecular nanometer tubes that extends through the crystal. Upon complexation of telmisartan with copper(II) ion, the antihypertensive effects of the pharmaceutical is retained and the antimicrobial effects of the metal against *S. aureus* are improved. Furthermore, the antioxidant activity against superoxide anion and the cytotoxic effect against human lung and prostate cancer cell lines are improved by complexation. On the grounds of the biological results, described in this paper, we can infer that the complexation of the antihypertensive medication generates beneficial properties such as the enhancement of the antioxidant activity, the cytotoxic behavior against lung and prostate cancer, retaining the original pharmaceutical properties, and the antibacterial effect against *S. aureus*.

■ ASSOCIATED CONTENT

Ⓢ Supporting Information

Tables of fractional coordinates and equivalent isotropic displacement parameters of the non-H atoms (Table S1), full bond distances and angles (Table S2), atomic anisotropic displacement parameters (Tables S3), and hydrogen atoms positions (Tables S4). This material is available free of charge via the Internet at http://pubs.acs.org.

■ AUTHOR INFORMATION

Corresponding Author

*Fax: +542214259485. E-mail: williams@quimica.unlp.edu.ar.

Notes

The authors declare no competing financial interest.

■ ACKNOWLEDGMENTS

This work was supported by UNLP, UNCAUS, CONICET (PIP 1529), SAF2010-16198, CICPBA, and ANPCyT (PME06 2804 and PICT06 2315), Argentina. E.G.F., G.A.E., and O.E.P. are research fellows of CONICET. P.A.M.W. is a research fellow of CICPBA, Argentina. M.S.I. and J.J.M.M. are fellowship holders from CONICET. We also thank Professor Guillermo Docena for providing us with a culture room.

■ REFERENCES

(1) de Gasparo, M.; Catt, K. J.; Inagami, T.; Wright, J. W.; Unger, Th. *Pharmacol. Rev.* **2000**, *52*, 415−472.
(2) Battershill, A. J.; Scott, L. J. *Drugs* **2006**, *66*, 51−83.
(3) Schmieder, R. E. *Am. J. Hypertension* **2005**, *18*, 720−730.
(4) Chrysan, S. G. *Clin. Therapeut.* **2008**, *30*, 2181−2190.
(5) Maeda, A.; Okazaki, T.; Inoue, M.; Kitazono, T.; Yamasaki, M.; Lemonnier, F. A.; Ozaki, S. *Int. Immunopharmacol.* **2009**, *9*, 1183−1188.
(6) Ferrario, C. M. *Am. J. Hypertens.* **2002**, *15*, 9S−13S.
(7) Arafat, H. A.; Gong, Q.; Chipitsyna, G.; Rizvi, A.; Saa, C. T.; Yeo, C. J. *J. Am. Coll. Surg.* **2007**, *204*, 996−1006.
(8) Solomon, E. I.; Lowery, M. D. *Science* **1993**, *259*, 1575−1581.
(9) Cass, A. E.; Hill, H. A. *Ciba Found. Symp.* **1980**, *79*, 71−91.
(10) Ibrahim, M.; Wang, F.; Lou, M.; Xie, G.; Li, B.; Bo, Z.; Zhang, G.; Liu, H. A. *J. Biosc. Bioeng.* **2011**, *112*, 570−576.
(11) Etcheverry, S. B.; Williams, P. A. M. New developments in medicinal chemistry. In Ortega, M. P., Gil, I. C., Eds.; *Medicinal Chemistry of Copper and Vanadium Bioactive Compounds*; Nova Science: Hauppauge, 2009; pp 105−129.
(12) Denadai, Â.M.L.; de Oliveira, A. M.; Daniel, I. M. P.; Carneiro, L. A.; Ribeiro, K. C.; Beraldo, H. O.; da Costa, K. J. R.; da Cunha, V. C.; Cortés, M. E.; Sinisterra, R. D. *Supramolec. Chem.* **2012**, *24*, 204−212.
(13) de Paula, W. X.; Denadai, Â.M.L.; Santoro, M. M.; Braga, A. N. G.; Santos, R. A. S.; Sinisterra, R. D. *Int. J. Pharm.* **2011**, *404*, 116−123.
(14) Etcheverry, S. B.; Ferrer, E. G.; Naso, L.; Barrio, D. A.; Lezama, L.; Rojo, T.; Williams, P.A. M. *Bioorg. Med. Chem.* **2007**, *15*, 6418−6424.
(15) Etcheverry, S. B.; Di Virgilio, A. L.; Nascimento, O. R.; Williams, P. A. M. *J. Inorg. Biochem.* **2012**, *107*, 25−33.
(16) Islas, M. S.; Rojo, T.; Lezama, L.; Griera Merino, M.; Cortes, M. A.; Rodriguez Puyol, M.; Ferrer, E. G.; Williams, P. A. M. *J. Inorg. Biochem.* **2013**, *123*, 23−33.
(17) *WINEPR SimFonia*, Vol. *25*, Bruker Analytische Messtecnik GmbH: Karlsruhe, 1996.
(18) *CrysAlisPro*, version 1.171.33.48 (release 15-09-2009 CrysAlis171.NET); Oxford Diffraction Ltd.: Oxfordshire, 2009.
(19) Zhao, J.; Mi, L.; Hu, J.; Hou, H.; Fan, Y. *J. Am. Chem. Soc.* **2008**, *130*, 15222−15223.
(20) G. M. Sheldrick *SHELXL-97. Program for Crystal Structures Analysis*; University of Göttingen: Göttingen, Germany, 1997.
(21) Sheldrick, G. M. *Acta Crystallogr. A* **2008**, *64*, 112−122.
(22) Van der Sluis, P.; Spek, A. L. *Acta Crystallogr., Sect. A* **1999**, *46*, 194−201.
(23) Spek, A. L. *PLATON, A Multipurpose Crystallographic Tool*; Utrecht University: Utrecht, The Netherlands, 1998.
(24) Diez-Marques, M. L.; García-Escribano, C.; Medina, J.; Boyano-Adanez, M. C.; Arilla, E.; Torrecilla, G.; Rodriguez-Puyol, D.; Rodriguez-Puyol, M. *Endocrinology* **1995**, *136*, 3444−3451.
(25) Cariaga-Martinez, A. E.; López-Ruiz, P.; Nombela-Blanco, M. P.; Motiño, O.; González-Corpas, A.; Rodriguez-Ubreva, J.; Lobo, M. V.; Cortés, M. A.; Colás, B. *Cell Signal.* **2013**, *25*, 1586−1597.
(26) Luo, C.; Li, Y.; Zhou, B.; Yang, L.; Li, H.; Feng, Z.; Li, Y.; Long, J.; Liu, J. *Apoptosis* **2014**, *19*, 542−553.
(27) Calleros, L.; Lasa, M.; Rodríguez-Alvarez, F. J.; Toro, M. J.; Chiloeches, A. *Apoptosis* **2006**, *7*, 1161−1173.
(28) Del Nogal, M.; Luengo, A.; Olmos, G.; Lasa, M.; Rodriguez-Puyol, D.; Rodriguez-Puyol, M.; Calleros, L. *Apoptosis* **2012**, *17*, 1261−1274.
(29) Klančnik, A.; Piskernik, S.; Jeršek, B.; Smole Možina, S. *J. Microbiol. Methods* **2010**, *81*, 121−126.
(30) Suksrichavalit, T.; Prachayasittikul, S.; Nantasenamat, C.; Isarankura-Na-Ayudhya, C.; Prachayasittikul, V. *Eur. J. Med. Chem.* **2009**, *44*, 3259−3265.
(31) Berahou, A.; Auhmani, A.; Fdil, N.; Benharref, A.; Jana, M.; Gadhi, C. A. *J. Ethnopharm.* **2007**, *112*, 426−429.
(32) Rowe, F.; Vargas Superti, S.; Machado Scheibe, R.; Gomes Dias, C. *Diagn. Microbiol. Infect. Dis.* **2002**, *43*, 45−48.
(33) Johnson, C. K. *ORTEP-II. A Fortran Thermal-Ellipsoid Plot Program*; Report ORNL-5318; Oak Ridge National Laboratory, Oak Ridge, Tennessee, USA, 1976.
(34) Nakamoto, K. *Infrared and Raman Spectra of Inorganic and Coordination Compounds*, Part B, 5th ed.; Wiley: New York, 1997.
(35) Lin-Vien, D.; Colthup, N. B.; Fateley, W. G.; Grasselli, J. G. *The Handbook of Infrared and Raman Characteristic Frequencies of Organic Molecules*; Academic Press: Boston, 1991.
(36) Sampath, A.; Raghupathi Reddy, A.; Yakambaram, B.; Thirupathi, A.; Prabhakar, M.; Pratap Reddy, P.; Prabhakar Reddy, V. *J. Pharm. Biomed. Anal.* **2009**, *50*, 405−412.
(37) Franca, C. A.; Etcheverry, S. B.; Pis Diez, R.; Williams, P. A. M. *J. Raman Spectrosc.* **2009**, *40*, 1296−1300.
(38) Islas, M. S.; Franca, C. A.; Etcheverry, S. B.; Ferrer, E. G.; Williams, P. A. M. *J. Vib. Spectrosc.* **2012**, *62*, 143−151.
(39) Morgan, K. J. *J. Chem. Soc.* **1961**, 2343−2347.

(40) Gudasi, K. B.; Shenoy, R. V.; Vadavi, R. S.; Patil, M. S.; Patil, S. A.; Hanchinal, R. R.; Desai, S. A.; Lohithaswa, H. *Bioinorg. Chem. Appl.* **2006**, *2006*, 1−8.
(41) Wolff, H.; Müller, H.; Wolff, E. *J. Chem. Phys.* **1976**, *64*, 2192−2196.
(42) Antony, J.; von Helden, G.; Meijer, G.; Schmidt, B. *J. Chem. Phys.* **2005**, *123*, 014305−014315.
(43) Hathaway, B. J.; Billing, D. E. *Coord. Chem. Rev.* **1970**, *5*, 143−207.
(44) Latif Abuhijleh, A. *J. Mol. Struct.* **2010**, *980*, 201−207.
(45) Stokowa-Sołtys, K.; Jeżowska-Bojczuk, M. *J. Inorg. Biochem.* **2013**, *127*, 73−78.
(46) Lopes de Miranda, J.; Felcman, J. *Polyhedron* **2003**, *22*, 225−233.
(47) Peisach, J.; Blumberg, W. E. *J. Pharm. Biomed. Anal.* **2009**, *50*, 405−412.
(48) Xie, Y.; Bu, W.; Chan, A. S. C.; Xu, X.; Liu, Q.; Zhang, Z.; Yu, J.; Fan, Y. *Inorg. Chim. Acta* **2000**, *310*, 257−260.
(49) Nakai, M.; Sekiguchi, F.; Obata, M.; Ohtsuki, C.; Adachi, Y.; Sakurari, H.; Rehder, D.; Yano, S. *J. Inorg. Biochem.* **2005**, *99*, 1275−1282.
(50) Ohno, K.; Amano, Y.; Kakuta, H.; Niimi, T.; Takakura, S.; Orita, M.; Miyata, K.; Sakashita, H.; Takeuchi, M.; Komuro, I.; Higaki, J.; Horiuchi, M.; Kim-Mitsuyama, S.; Mori, Y.; Morishita, R.; Yamagishi, S. *Biochem. Biophys. Res. Commun.* **2011**, *404*, 434−437.
(51) Grossman, E. *Diabetes Care* **2008**, *31*, S185−S189.
(52) Fukai, T.; Ushio-Fukai, M. *Antioxid. Redox Signal* **2011**, *15*, 1583−1606.
(53) Santini, C.; Pellei, M.; Gandin, V.; Porchia, M.; Tisato, F.; Marzano, C. *Chem. Rev.* **2014**, *114*, 815−862.
(54) Trávniček, Z.; Vančo, J.; Hošek, J.; Buchtík, R.; Dvořák, Z. *Chem. Central J.* **2012**, *6*, 160−172.
(55) Kruszewska, H.; Zareba, T.; Tyski, S. *Acta Polym. Pharm.* **2012**, *69*, 1368−1371.
(56) Tanaka, J. C. A.; da Silva, C. C.; de Oliveira, A. J. B.; Nakamura, C. V.; Dias Filho, B. P. *Braz. J. Med. Biol. Res.* **2006**, *39*, 387−391.
(57) Urquiza, N. M.; Islas, M. S.; Dittler, M. L.; Moyano, M. A.; Manca, S. G.; Lezama, L.; Rojo, T.; Martínez Medina, J. J.; Diez, M.; López Tévez, L.; Williams, P. A. M.; Ferrer, E. G. *Inorg. Chim. Acta* **2013**, *405*, 243−251.
(58) Marshall, T. G.; Fenter, B.; Marshall, F. E. *J. Indep. Med. Res.* **2004**, *2*, 1−9.
(59) Servant, G.; Escher, E.; Guillemette, G. *Regul. Pept.* **1998**, *73*, 35−41.